Low-Noise 0.8–0.96- and 0.96–1.12-THz Superconductor–Insulator–Superconductor Mixers for the Herschel Space Observatory

Brian D. Jackson, Gert de Lange, Tony Zijlstra, Matthias Kroug, Jacob W. Kooi, Jeffrey A. Stern, and Teun M. Klapwijk

Abstract—Heterodyne mixers incorporating Nb SIS junctions and NbTiN–SiO$_2$–Al microstrip tuning circuits offer the lowest reported receiver noise temperatures to date in the 0.8–0.96- and 0.96–1.12-THz frequency bands. In particular, improvements in the quality of the NbTiN ground plane of the SIS devices' on-chip microstrip tuning circuits have yielded significant improvements in the sensitivity of the 0.96–1.12-THz mixers relative to previously presented results. Additionally, an optimized RF design incorporating a reduced-height waveguide and suspended stripline RF choke filter offers significantly larger operating bandwidths than were obtained with mixers that incorporated full-height waveguides near 1 THz. Finally, the impact of junction current density and quality on the performance of the 0.8–0.96-THz mixers is discussed and compared with measured mixer sensitivities, as are the relative sensitivities of the 0.8–0.96- and 0.96–1.12-THz mixers.

Index Terms—Astronomical satellites, niobium, niobium compounds, radio astronomy, submillimeter-wave mixers, superconductor–insulator–superconductor (SIS) mixers.

I. INTRODUCTION

THE heterodyne instrument for the far-infrared (HIFI) [1],[1] is a high-sensitivity, high-resolution heterodyne spectrometer that is being built for the European Space Agency's Herschel Space Observatory [2].[2] The instrument's 0.48–1.25- and 1.41–1.91-THz frequency coverage will offer astronomers an unprecedented opportunity to observe a significant fraction of the submillimeter and far-infrared spectrum, much of which is not observable from ground-based telescopes due to absorption by atmospheric water vapor. In order to take full advantage of this space-based observatory, the HIFI instrument will incorporate state-of-the-art cryogenic heterodyne mixers, with five superconductor–insulator–superconductor (SIS) mixers covering the 0.48–1.25-THz band and two hot-electron bolometer (HEB) mixers covering 1.41–1.91 THz.

Unfortunately, although traditional Nb SIS mixers offer quantum-limited sensitivities below 0.7 THz [3]–[5], increasing resistive losses in their Nb-based microstrip transmission lines at frequencies above the "gap frequency" of Niobium ($F_{\mathrm{gap,Nb}} = 2\Delta_{\mathrm{Nb}}/h \sim 0.7$ THz) [6] cause the sensitivities of these mixers to drop significantly above 0.7 THz [7]. However, previous work has shown that the use of NbTiN-based[3] microstrip RF tuning circuits allows the sensitivity of 0.75–1.0-THz SIS mixers to be significantly improved [8]–[10]. Furthermore, as is discussed in more detail in [11], the integration of Nb SIS junctions with a NbTiN–SiO$_2$–Al microstrip tuning circuit in which the NbTiN ground plane is deposited at 400 °C (in place of the room-temperature-deposited films used previously) allows low-noise SIS mixer operation to be extended to at least 1.12 THz.

Following from these advances, this paper describes the RF design and performance of the 0.8–0.96- and 0.96–1.12-THz mixers that have been developed for use in Bands 3 and 4 of the HIFI instrument. In particular, this paper discusses the integrated designs of reduced-height waveguide embedding circuits and two-junction SIS tuning circuits that yield efficient coupling of radiation to the mixers' SIS junctions over each frequency band. Additionally, the impact of the current densities and leakage currents of the SIS junctions on their mixing performance is discussed in light of simulations of the heterodyne performance of the mixers' two-junction tuning circuits. This mixer model is also used to compare the relative performance of the 0.8–0.96- and 0.96–1.12-THz mixers.

The optomechanical designs of these mixers (including their corrugated horns), in addition to the designs of their intermediate frequency (IF) output coupling circuits and their shielding from external electromagnetic interference, are described elsewhere [12].

B. D. Jackson is with the SRON National Institute for Space Research, 9747 AD Groningen, The Netherlands and also with the Kavli Institute of Nanoscience, Faculty of Applied Sciences, Delft University of Technology, 2628 CJ Delft, The Netherlands (e-mail: B.D.Jackson@sron.rug.nl).

G. de Lange is with the SRON National Institute for Space Research, 9747 AD Groningen, The Netherlands (e-mail: G.de.Lange@sron.rug.nl).

T. Zijlstra, M. Kroug, and T. M. Klapwijk are with the Faculty of Applied Sciences, Kavli Institute of Nanoscience, Delft University of Technology, 2628 CJ Delft, The Netherlands (e-mail: zijlstra@dimes.tudelft.nl; kroug@dimes.tudelft.nl; t.m.klapwijk@tnw.tudelft.nl).

J. W. Kooi is with the California Institute of Technology, Pasadena, CA 91125 USA (e-mail: kooi@submm.caltech.edu).

J. A. Stern is with the Jet Propulsion Laboratory, California Institute of Technology, Pasadena, CA 91109 USA (e-mail: Jeffrey.Stern@jpl.nasa.gov).

Digital Object Identifier 10.1109/TMTT.2005.862717

[1][Online]. Available: www.sron.nl/divisions/lea/hifi
[2][Online]. Available: http://www.rssd.esa.int/herschel

[3]For simplicity, the compound Nb$_{1-x}$Ti$_x$N$_{1-\delta}$, where $x = 0.3$ and $\delta \cong 0$, is referred to as NbTiN throughout this paper.

II. Mixer and SIS Device Design

Previous reports of the development of NbTiN-based SIS mixers made use of two basic mixer geometries: a quasi-optical mixer incorporating a 0.95-THz twin-slot antenna (see [9]) and a waveguide mixer incorporating a full-height 1-THz waveguide (see [10]). These results demonstrated that a NbTiN–SiO$_2$–Al microstrip RF matching network can be integrated with "standard" 1-μm^2 Nb–Al-AlO$_x$–Nb SIS junctions to yield low receiver noise temperatures up to 1 THz (and [11] demonstrates that this region of low-noise operation may be extended to at least 1.12 THz by the use of an NbTiN ground plane that is deposited at 400 °C). However, the fixed-tuned RF bandwidth of the 1-THz waveguide mixer in [10] was limited to ∼100 GHz, whereas the quasi-optical mixer in [10] offered fixed-tuned bandwidths of ∼200 GHz. This limitation of the previously demonstrated waveguide mixer has been addressed by a redesign of the waveguide embedding geometry [13] and the SIS device's on-chip microstrip tuning circuit to optimize the coupling to the SIS junctions.

The starting point of this redesign (see [14]) was a move from the full-height 1-THz waveguide geometry that was used in [10] to scaled versions of the 0.65-THz half-height waveguide geometry that was used in mixers produced for the James Clerk Maxwell Telescope in Hawaii [15], [16]. In particular, for each of these designs, Fig. 1(a) presents the effective source impedance at the input to the on-chip microstrip tuning circuit that is produced by a combination of the waveguide, the fixed-depth waveguide backshort, the fused quartz substrate in the substrate channel (including the RF choke filter on the substrate), and the "across-the-waveguide" bowtie probe. (This "source impedance" has been calculated in a three-dimensional (3-D) electromagnetic field simulator.[4]) From this plot, it is seen that the original 1-THz waveguide design is characterized by a source impedance with a strong frequency dependence and a large imaginary component. In comparison, the source impedances of the 0.65- and 0.88-THz half-height waveguide designs are much less frequency dependent (although they retain significant reactive components). These results are consistent with those obtained previously in [17] and [18], both in theoretical calculations and in experiment.

As was also demonstrated in [18], further "improvements" in the source impedance offered by the waveguide embedding design are obtained by suspending the SIS device substrate in the substrate channel (and fine-tuning the dimensions in the RF choke filter to recenter the passband of the filter on the center frequency of the design). As is seen in Fig. 1(b), this further reduces the frequency dependence and reactance of the source impedance at the input of the on-chip tuning circuit. (For clarity, only the results for the 0.88-THz design are shown here—the 1.04-THz design is a scaled version of the 0.88-THz design.)

Fig. 2 illustrates the geometry of the 0.88-THz suspended substrate waveguide geometry that is used in the devices described here. The critical waveguide and device substrate dimensions in this design are summarized in Table I. Three-dimensional electromagnetic simulations of the embedding impedance offered by the waveguide geometries are calculated
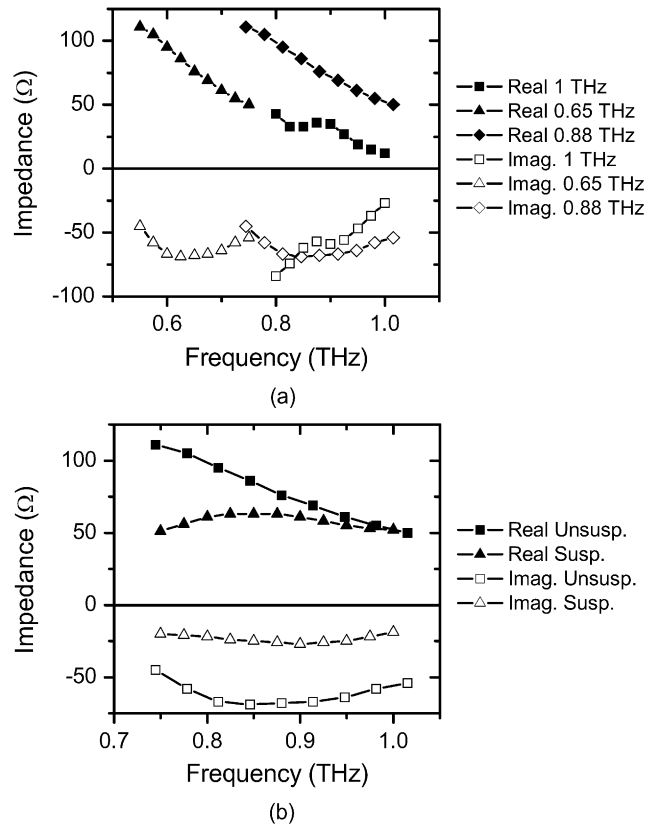
[4]Ansoft Corporation, Pittsburgh, PA.

Fig. 1. Effective source impedance at the input to the on-chip microstrip tuning circuit (at the center of the "across-the-waveguide" bowtie probe, given the fixed-depth waveguide backshort, the fused quartz substrate in the substrate channel, and the RF choke filter patterned on the substrate surface). (a) Comparison of the full-height 1-THz waveguide geometry and the half-height 0.65-THz waveguide geometries used previously with the "unsuspended" half-height 0.88-THz design. (b) Comparison of half-height 0.88-THz waveguide geometries with suspended and unsuspended quartz substrates in the substrate channel. The geometries of the mixers analyzed here are summarized in Fig. 2 and Table I.

for a reference plane at the center of the bowtie waveguide probe (i.e., at the input to the on-chip microstrip tuning circuit). The 1.04-THz mixer design that is used here is a scaled version of the 0.88-THz design.

Finally, the RF designs of the mixers were completed by optimizing the geometry of the twin-junction tuning circuit used in [10] (see Fig. 3) to maximize the coupling of incident RF power to the SIS junctions over the 0.8–0.96 and 0.96–1.12-THz bands, given the frequency-dependent source impedances in Fig. 1. The resulting coupling to the SIS junctions is plotted in Fig. 4 for several combinations of waveguide embedding geometry and SIS device parameters (which are summarized in Tables I and II, respectively).

A number of features are clearly identifiable in these results. First, it is seen that, with a moderate junction current density ($J_c = 8$ kA/cm^2), the "suspended" and "unsuspended" 0.88-THz designs offer similar coupling efficiencies (50%–60% across the 0.8–0.96-THz band, with the "unsuspended" design actually offering slightly higher efficiencies). Moving to a higher current density ($J_c = 15$ kA/cm^2) significantly improves the coupling to the junctions (due to the junctions' reduced ωRC product), and the coupling obtained with the "suspended" design is slightly better than that obtained with the
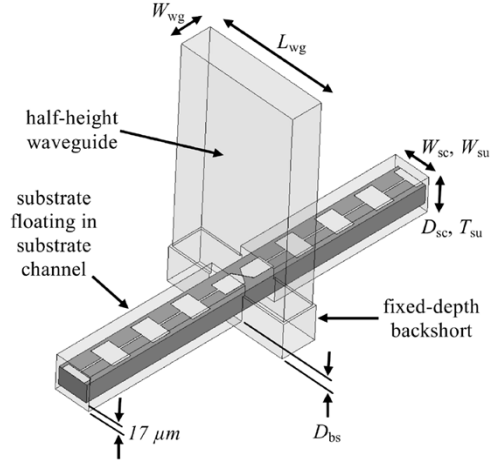
Fig. 2. Suspended substrate waveguide geometry incorporating a half-height waveguide with a bowtie waveguide probe located at the center of the waveguide and a four-section RF choke filter in the substrate channel. The dimensions of the waveguide, substrate channel, and substrate are summarized in Table I. The reference plane at which the embedding impedances are calculated for this structure is located at the center of the bowtie waveguide probe. In other words, this reference plane is located at the input of the on-chip microstrip tuning circuit that is seen in Fig. 3. Ground and dc/IF connections to the SIS device are made by wire-bonding to gold pads at the two ends of the device (beyond the left and right edges of this figure).

TABLE I
WAVEGUIDE MIXER EMBEDDING GEOMETRIES ANALYZED IN FIG. 1

Design	waveguide $W_{wg} \times H_{wg}$	backshort depth D_{bs}	substrate channel $W_{sc} \times D_{sc}$	substrate [b] $W_{su} \times T_{su}$
1 THz	120 x 240	60	90 x 75	70 x 40
650 GHz	100 x 400	80	100 x 75	80 x 40
0.88 THz	74 x 296 [a]	60	75 x 55	60 x 30
0.88 THz suspended	74 x 296 [a]	25	90 x 87	75 x 45 [c]

all dimensions are given in μm, W = width, D = Depth, H = Height
[a] dimensions used in modeling, actual dimensions are 75 μm x 300 μm and 60 μm x 240 μm
[b] polished fused quartz, ε_r = 3.8, T_{su} = the substrate thickness after thinning (by polishing)
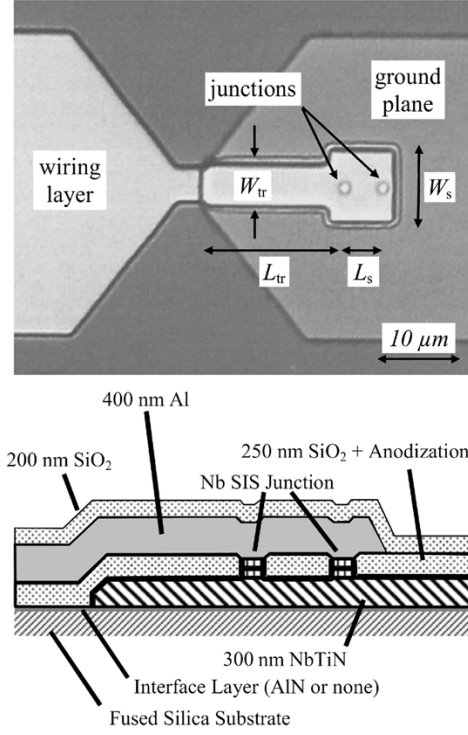[c] suspended by 17 μm above the bottom of the substrate channel

Fig. 3. Twin-junction SIS tuning circuit geometry. Top: photograph of a 1-THz mixer device (adapted from [10]). Note that the dimensions of the microstrip tuning circuit in this image are slightly different than those in the devices used here, but that the basic geometry is the same. Bottom: schematic cross section of the tuning circuit layer structure (adapted from [9]). The dimensions of the microstrip tuning circuit are summarized in Table II.

tunnel junctions with $A \sim 1~\mu m^2$. The microstrip transmission lines combine a 300-nm NbTiN ground plane, a 250-nm SiO$_2$ dielectric layer (with a nominal $\varepsilon_r = 3.8$), and a 400-nm Al wiring layer (with a low-temperature dc resistivity of $\rho_{Al,4K} = 0.3$–$0.5~\mu\Omega \cdot cm$).

The fabrication and performance of these mixers are described and discussed further in the following sections.

III. SIS DEVICE FABRICATION

The SIS devices used here were produced using a process that is derived from that which was used for the demonstrations of quasi-optical and waveguide mixers incorporating NbTiN/SiO$_2$/Al tuning circuits (see [9] and [10], respectively). However, a number of significant modifications to the process have been made in order to improve the patterning of the SIS junctions and the Al wiring layer, and to incorporate higher-quality NbTiN ground planes in the 1.04-THz mixers.

The primary modifications to the junction definition process have been: 1) to move from a CF$_4$+O$_2$ gas mixture to SF$_6$+O$_2$ for the reactive ion etching of the Nb junction electrodes (to improve the anisotropy and repeatability of the etch) and 2) to add an O$_2$ plasma etch of the resist pattern following the etch of the top Nb junction electrode (prior to Ar sputter etching the Al-AlO$_x$ barrier and reactive ion etching the bottom Nb electrode). As is discussed in [11], this "resist recessing" step yields a stepped junction profile in which the edges of the active portion of the Al-AlO$_x$ barrier are not exposed to the Ar sputter etch of the barrier, since the final size of the top electrode is reached

"unsuspended" design. Beyond this, Fig. 4(b) demonstrates that the coupling to the junctions in the 1.04-THz design is strongly dependent upon the properties of the NbTiN ground plane—the use of a film deposited at room temperature is expected to result in a strong drop in coupling above ~1 THz (see [9] and [10]), whereas the use of a film deposited at 400 °C should offer strong coupling over the full 0.96–1.12-THz band (see [11]).

Based upon these calculations, SIS mixers with three combinations of junction current density, NbTiN quality (superconducting transition temperature, $T_{c,NbTiN}$, and low-temperature normal-state resistivity, $\rho_{n,20K}$), and embedding geometry have been produced. Two 0.88-THz mixers (incorporating junctions with $J_c = 6.5$ and 13 kA/cm^2, $T_{c,NbTiN} = 14.4$ K, $\rho_{n,20K} = 110\mu\Omega \cdot cm$ and a suspended embedding geometry) have been produced for Band 3 of the HIFI instrument. Similarly, a 1.04-THz mixer incorporating a suspended-substrate waveguide geometry with $J_c = 6.5$ kA/cm^2, $T_{c,NbTiN} = 16$ K, and $\rho_{n,20K} = 60\mu\Omega \cdot cm$ has been produced for Band 4 of the HIFI. In all cases, the SIS junctions are Nb/Al-AlO$_x$/Nb
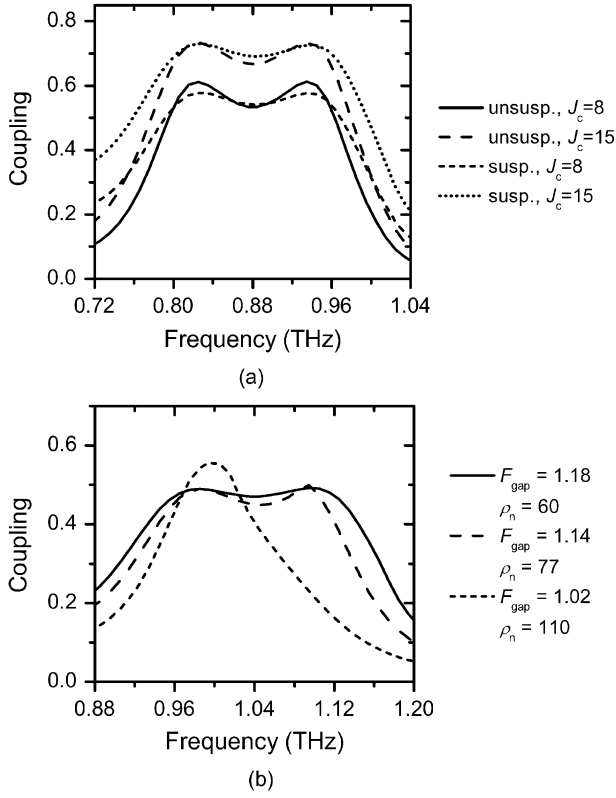
(a)

(b)

Fig. 4. (a) Calculated coupling to the SIS junctions for twin-junction SIS devices mounted in half-height 0.88-THz waveguides with suspended and unsuspended substrates. A slight benefit is obtained from the suspended substrate design if high current-density junctions are used (the values of J_c in the legend are given in kA/cm^2). (b) Calculated coupling to suspended-substrate twin-junction SIS devices mounted in a half-height 1.04-THz waveguide. A clear dependence of the RF coupling on the superconducting properties of the NbTiN ground plane is observed. Note that the values given the legends are the "gap frequency" and low-temperature normal-state resistivity of NbTiN in-THz and $\mu\Omega \cdot$ cm, respectively ($F_{\mathrm{gap,NbTiN}} = 2\Delta_{\mathrm{NbTiN}}/h$).

TABLE II
SIS JUNCTION AND NbTiN GROUND-PLANE CHARACTERISTICS AND TUNING
CIRCUIT GEOMETRIES OF THE SIS DEVICES DISCUSSED HERE

Wafer Label	880 low-J_c	880 high-J_c	1040
Device Number[a]	c78-A, c87-A	c20-B, c78-B	c22-C, f49-C
Waveguide	0.88 THz	0.88 THz	1.04 THz
Embedding Design	suspended	suspended	suspended
Junction			
A (μm^2)	0.9, 1.1	0.9	1.15, 1.05
J_c (kA/cm^2)	6.5	13	6.5
$R_{2.0\mathrm{mV}}/R_N$	60	20	30-50
NbTiN			
$T_{\mathrm{deposition}}$ (ºC)	20	20	400
T_c (K)	14.4	14.4	16
$\rho_{\mathrm{n,20K}}$ ($\mu\Omega \cdot$cm)	110	110	60
Separation			
L_s (μm)	5.5	5.5	5.5, 3.5
W_s (μm)	6-7	6-7	6-7
Transformer			
L_{tr} (μm)	24, 27	24	22, 20
W_{tr} (μm)	5-6	5-6	4, 5

[a] Note that the first letter/number combination identifies a specific device on the mask layout, while the suffix (A,B,C) is used to distinguish between different wafers. Wafer C uses one mask layout while wafers A and B use a common mask design (thus, c78-A and c78-B have the same geometries, other than fabrication tolerances).

at the completion of the bottom electrode etch. This is expected to improve the quality of a typical junction (i.e., to reduce its leakage current) by reducing the risk of damage to the tunnel barrier during the etch process.

On top of these changes to the junction definition step, the other significant changes to the SIS device process have been: 1) using a chlorine-based reactive ion etch to pattern the Al wiring layer (which offers improved dimension control relative to the lift-off process that was used in [9] and [10]) and 2) using NbTiN ground planes deposited at 400 °C (at the Jet Propulsion Laboratory [19]) in the 1.04-THz mixers. Finally, because the lift-off process that was used previously cannot be used to pattern ground planes that are deposited at high temperatures, these films were patterned by reactive ion etching in SF$_6$ + O$_2$.

As in [9] and [10], contact UV lithography is used for all resist pattern definition, RF magnetron sputtering is used to deposit the SiO$_2$ dielectric and passivation layers, and dc magnetron sputtering is used to deposit the Nb, NbTiN, and Al layers.

Table II summarizes the material characteristics and tuning circuit geometries of the SIS devices that are discussed in the Sections that follow.

IV. DC CURRENT–VOLTAGE CHARACTERISTICS

Fig. 5 presents the bias current and IF output power as a function of bias voltage for two SIS devices (one 0.88-THz device with $J_c = 13$ kA/cm^2 and one 1.04-THz device with $J_c = 6.5$ kA/cm^2). In general, the junction qualities of these devices, as measured by their subgap to normal-state resistance ratios $(R_{2.0\,\mathrm{mV}}/R_N)$, are excellent, with $R_{2.0\,\mathrm{mV}}/R_N = 30–60$ for devices with $J_c = 6.5$ kA/cm^2 and $R_{2.0\,\mathrm{mV}}/R_N \sim 20$ for devices with $J_c = 13$ kA/cm^2 (at a mixer temperature of 2–2.5 K).

Beyond this, two other features are noted in Fig. 5. First, the photon step in the 1.04-THz device pumped at 1.14 THz is barely wide enough to yield a bias point that is not affected by the Shapiro effect (which can cause instabilities in the IF output power in the output power peaks seen on either side of $V_{\mathrm{Shapiro}} = hF_{\mathrm{LO}}/2e = 2.1$ mV/THz). Additionally, whereas the 0.88-THz devices have a typical series resistance in their Al wiring layer of 0.7 Ω (which is consistent with the low-temperature dc resistivity of the Al film), the 1.04-THz devices have a series resistance of 1.5 Ω. Note that the resistivity of the Al layer was determined from the resistance of long, narrow strips of Al deposited under the same conditions as the Al in the actual devices, while the the series resistance in the Al wiring of actual junctions is determined from the slope in the junctions' zero-voltage supercurrents. The higher series resistance in the 1.04-THz devices indicates that the resistivity of the Al wiring layer is higher in the 1.04-THz devices than the $\sigma_{\mathrm{Al,4K}} \sim 0.5\,\mu\Omega \cdot$ cm that is assumed in the design. This is not fully understood, but is thought to be related to the fact that the surface of the SiO$_2$ dielectric layer on which the Al is deposited is significantly rougher in the 1.04-THz devices than in the 0.88-THz devices (due to differences in the growth mechanics of SiO$_2$ layers on NbTiN films deposited at 400 °C and room temperature).
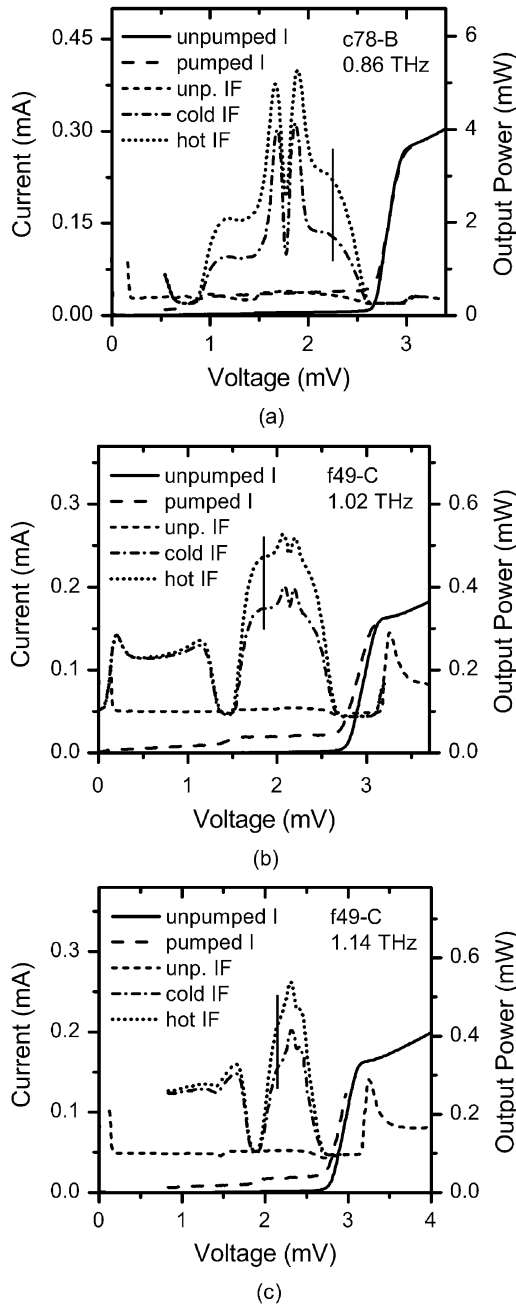
Fig. 5. (a) Bias current and mixer IF output power as a function of bias voltage for a 0.88-THz SIS tunnel junction with a current density of $J_c = 13$ kA/cm^2, operated at 0.86 THz. (b) and (c) Bias current and mixer IF output power as a function of bias voltage for a 1.04-THz SIS junction with $J_c = 6.5$ kA/cm^2, operated at 1.02 THz [in (b)] and 1.14 THz [in (c)]. The limited bias range that remains in the 1.04-THz device pumped at 1.14 THz is noted—this is close to the maximum operating frequency for a "traditional" Nb/Al-AlO$_x$/Nb SIS junction. In both cases, the junction qualities (as measured by their subgap to normal-state resistance ratios) are excellent, with $R_{2.0\,\mathrm{mV}}/R_\mathrm{N} = 30$–60 and 20 obtained for $J_c = 6.5$ and 13 kA/cm^2, respectively. (Note that (b) is adapted from [11].) The vertical markers on the hot and cold IF output power characteristics in each plot indicate the bias voltage that is typically used for RF sensitivity testing—(a) indicates the bias voltage that is used for 0.88-THz mixers, while (b) and (c) indicate the bias voltages that are used for 1.04-THz mixers below 1.04 and above 1.14 THz, respectively (no LO is available in the gap between these ranges).

V. RF MEASUREMENT SETUP

The heterodyne sensitivities of the mixers described here have been obtained from conventional Y-factor measurements using
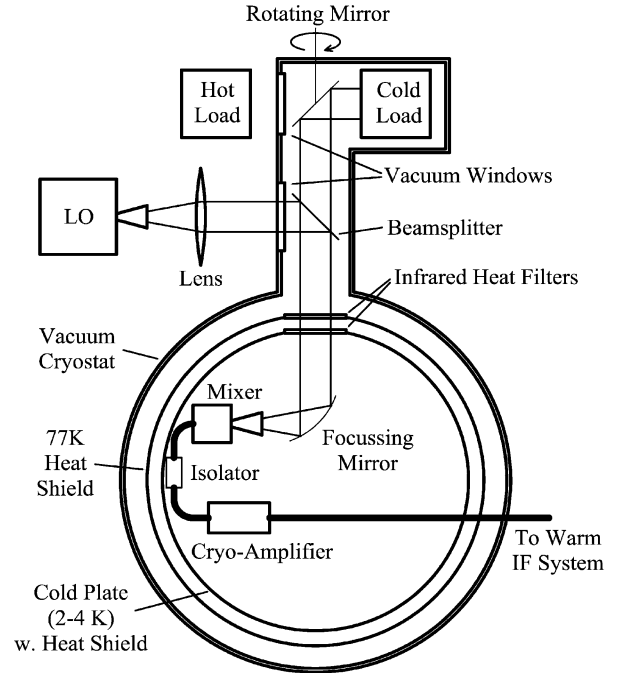

Fig. 6. Schematic representation of the mixer test receiver. This includes a vacuum hot–cold load that is used to improve the accuracy of measurements of the mixer sensitivity by removing the vacuum window from the optical path to the liquid-nitrogen-cooled cold load, and by eliminating the influence of atmospheric absorption of submillimeter radiation on the noise measurements.

a room-temperature "hot" blackbody signal source and a 77 K "cold" blackbody source (using the Callen–Welton formulation [20] to determine their effective source temperatures from their physical temperatures). Furthermore, because this work is focused on the development of mixers for the HIFI instrument (which includes a window-free, all-reflective optical design), an attempt has been made to minimize the receiver's input coupling losses by: 1) replacing the dielectric focusing lens used previously with a Au-coated mirror on the 4 K stage of the liquid-helium-cooled test cryostat and 2) making use of a vacuum hot–cold load. In particular, using this vacuum hot–cold load removes the cryostat's vacuum window from the optical path between the mixer and the cold load and eliminates the effect of absorption by atmospheric water vapor, which can be significant at submillimeter wavelengths. Fig. 6 presents a schematic representation of the mixer test system, including the vacuum hot–cold load, in which a rotating mirror located inside the cryostat is used to chop between the hot load (a room-temperature absorber located outside the cryostat) and the cold load. This cold load is produced by coating the bottom of a liquid nitrogen vessel in the receiver's vacuum system with a mixture of silicon carbide grains in black Stycast epoxy [21]. Previous measurements [22] showed that this coating has an emissivity of $\varepsilon \sim 0.95$ at submillimeter wavelengths.

Differences between the mixer test system and the environment of the HIFI instrument have been further minimized by the use of a cryogenic intermediate frequency (IF) amplification system that includes prototypes of the cryogenic 4–8-GHz isolator and low-noise amplifier used in the HIFI instrument (from PamTech,[5] and the Centro Astronomico de Yebes [23], respec-

tively). (The input noise temperature of this IF system is ~8 K, which is only slightly less than the expected 10 K noise of the IF chain in the HIFI instrument.) Furthermore, the SIS devices have been tested in prototypes of the mixer blocks that will be used in the instrument's 0.88- and 1.04-THz bands (see [12]), at an operating temperature of 2–2.5 K (which is close to the expected operating temperature of the mixers in the instrument). (This low operating temperature is reached by pumping on the cryostat's helium bath.)

In reporting the receiver sensitivities presented here, two values are generally given: $T_{\rm N,rec}$, the measured double side-band (DSB) receiver sensitivity obtained with the mixer mounted in the test receiver (using a power meter to detect the total output power over the 4–8-GHz IF band), and $T_{\rm N,mixer+IF}$, the effective input noise of the mixer and the IF amplifier system (which is obtained by correcting the measured receiver noise temperatures for the calculated/measured losses in the 14- or 49-μm Mylar beamsplitter and the Zitex G104 infrared heat-filters).

Finally, the mixers' direct-detection sensitivities are also presented here because they provide a snapshot of the frequency dependence of the coupling of radiation from an incident optical beam to the SIS junctions. These results have been obtained with a Fourier transform spectrometer in which an evacuated Michelson interferometer is used as a tunable signal source that is injected into the mixer test cryostat via the optical window through which the "hot" signal passes in heterodyne sensitivity measurements. In order to allow the measured results to be compared with the calculated coupling efficiencies, the measured spectra have been corrected for a standing wave in the output of the Michelson interferometer (with a period of ~70 GHz and a peak-to-peak amplitude of 0.8 dB) and have been multiplied by a factor of F (in THz) to account for the fact that the measured spectra are proportional to the photon detection efficiency, while the calculated spectra are of the power coupling.

VI. RF MEASUREMENT RESULTS

Fig. 7 presents the direct-detection sensitivities of several SIS devices in each of the three mixers discussed here (the 0.88-THz mixer with moderate- and high- J_c junctions and the 1.04-THz mixer with moderate- J_c junctions). From these results, it is seen that both current densities yield efficient coupling to the SIS junctions over broad RF bandwidths. Furthermore, provided that the response is properly centered on the target band (i.e., by properly matching the junction sizes to the tuning circuit geometries), efficient coupling can be obtained over the full 0.8–0.96- and 0.96–1.12-THz bands.

Following the direct-detection sensitivities, Fig. 8 presents measured heterodyne sensitivities of several of the SIS devices whose direct-detection sensitivities are plotted in Fig. 7. From these results, it is observed that the 0.88-THz mixers yield $T_{\rm N,rec} = 300$ K and $T_{\rm N,mixer+IF} = 200$ K, or better, across a significant fraction of the 0.8–0.96-THz band. The 1.04-THz mixers yield $T_{\rm N,rec} = 500$ K and $T_{\rm N,mixer+IF} = 400$ K, or better, across at least 1.03–1.15 THz (for a device tuned to this frequency range). Furthermore, a number of additional observations can be made: 1) the sensitivities of the 0.88-THz mixers
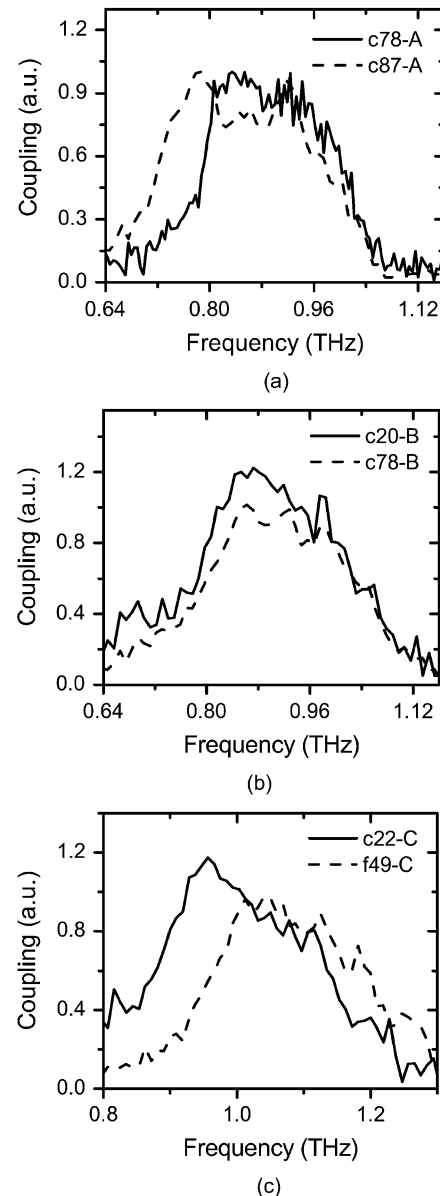
(a)

(b)

(c)

Fig. 7. Direct-detection sensitivities of several SIS devices mounted in the 0.88-THz and 1.04-THz mixer blocks, biased at $V_{\rm bias} = 2.4$–2.5 mV. In all cases, the embedding geometry is a half-height waveguide design with the substrate suspended in the substrate channel. (a) Results for 0.88-THz mixers with junction current densities of $J_c = 6.5$ kA/cm^2. (b) Results for 0.88-THz mixers with $J_c = 13$ kA/cm^2. (c) Results for 1.04-THz mixers with $J_c = 6.5$ kA/cm^2. In each case, strong coupling over a broad RF bandwidth is obtained (although the center-frequency and the frequency dependence of the response is dependent on the tuning circuit geometry and junction size). The geometries of these devices are summarized in Table II, using the device labels identified in the legend of each figure. Note that (c) is adapted from [11].

incorporating 6.5 and 13 kA/cm^2 junctions are similar (given the device-to-device variability in their sensitivities); 2) as is discussed further in [11], the use of an NbTiN ground plane deposited at 400 °C yields sensitive SIS mixers for frequencies up to at least 1.12 THz; and 3) the input noise temperatures of the 1.04-THz mixers are ~40%–50% higher than those of the 0.88-THz mixers. Note that receiver sensitivities have not been measured over the full bandwidths of the mxiers, due to a lack of LO power in some frequency bands (especially below 0.86 THz and between 1.04–1.14 THz). However, the
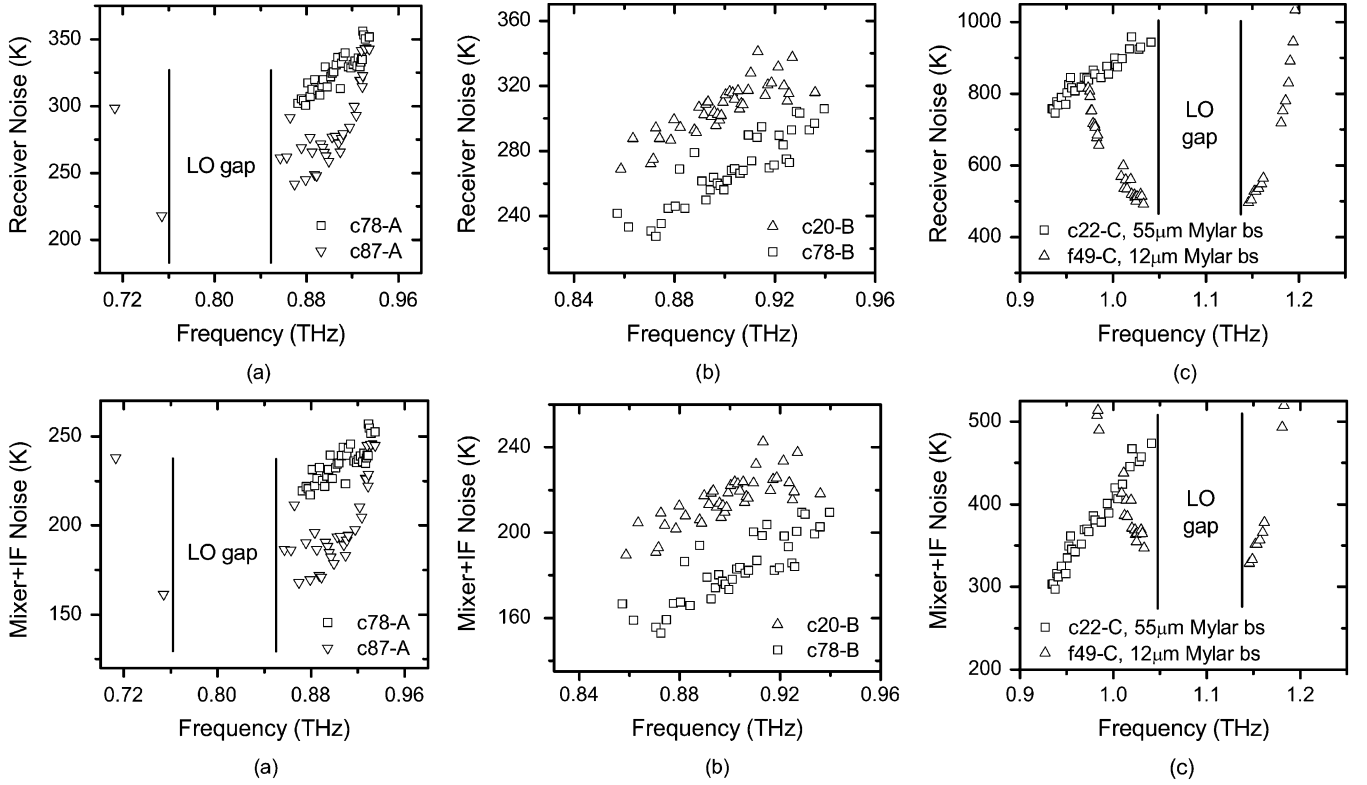
Fig. 8. Measured DSB receiver noise temperatures ($T_{\mathrm{N,rec}}$) for several of the devices/mixers whose direct detection (FTS) sensitivities are plotted in Fig. 7. At each frequency, the LO power level is adjusted to obtain optimum noise, while the bias voltage is held constant with frequency (at bias voltages that are indicated in Fig. 5). The effective input noise temperatures of the combination of the mixers and IF system ($T_{\mathrm{N,mixer+IF}}$) (obtained by correcting the measured receiver sensitivities for the calculated/measured losses in the receiver optics), are also shown. All of these measurements are performed at mixer temperatures of 2–2.5 K, averaging over the full bandwidth of a 4–8 GHz IF system with $T_{\mathrm{N,IF}} \sim 8$–10 K. (a) Results for 0.88-THz mixers with $J_c = 6.5$ kA/cm^2. (b) Results for 0.88-THz mixers with $J_c = 13$ kA/cm^2. (c) Results for 1.04-THz mixers with $J_c = 6.5$ kA/cm^2. In each case, high sensitivity over a broad RF bandwidth is obtained (although the center frequency and the frequency dependence of the response is dependent on the tuning circuit geometry and junction size). The geometries of these devices are summarized in Table II using the device labels indicated in the legends in the bottom right corner of each figure. Note that (c) is adapted from [11]. Note that the LO frequency ranges over which sensitivities are shown are limited by the tuning ranges of the Backward Wave Oscillators that are available. However, the direct detection spectral response curves of these devices, which are seen in Fig. 7, show that the coupling of incident radiation to the junctions over the relevant 0.8–0.96- and 0.96–1.12-THz bands is reasonably good.

direct-detection spectral response curves in Fig. 7 show that the coupling of incident radiation to the junctions remains reasonably efficient over the majority of the relevant 0.8–0.96- and 0.96–1.12-THz bands.

The determination of the DSB receiver conversion gains for these mixers was complicated by parasitic impedances in the mixers' IF output circuit, which introduced uncertainties to the use of the junction's unpumped shot-noise characteristics to calibrate the noise and gain of the receiver's IF system. However, despite these uncertainties, clear differences could be seen in the gains of the mixers from different wafers—c78-A offered $G_{\mathrm{rec,DSB}} \sim -8 \pm 1$ dB at 0.88 THz, c78-B offered $G_{\mathrm{rec,DSB}} \sim -4 \pm 1.5$ dB at 0.86 THz, and f49-C offered $G_{\mathrm{rec,DSB}} \sim -10 \pm 1$ dB at 1.04 THz.

The wider RF bandwidths that are expected from the use of higher current-density junctions (see Fig. 4) are not immediately obvious in the measured results in Figs. 7 and 8. However, this may be partly due to the 1-THz "gap frequency" of the NbTiN ground plane limiting the mixers' high-frequency performance (since the devices presented here have been selected to have strong responses in the 0.8–0.96- or 0.96–1.12-THz bands, as opposed to maximum bandwidth).

VII. DISCUSSION

A. Twin-Junction Mixer and Receiver Noise Model

Calculations of the coupling of radiation to the SIS junctions clearly show that the coupling efficiency increases significantly with increasing current-density (from $\sim 55\%$ at $J_c = 8$ kA/cm^2 to $\sim 70\%$ at $J_c = 15$ kA/cm^2 for the 0.88-THz mixer design). However, measurements of the heterodyne sensitivities of devices with $J_c = 6.5$ and 13 kA/cm^2 show no significant difference in performance. This may be attributed to the fact that the leakage currents of the higher current-density junctions are higher than those of the lower current-density junctions ($R_{2.0\mathrm{mV}}/R_N \sim 20$ in place of 30–60). In particular, the larger leakage currents apparently generate sufficient additional shot noise to counteract the improved coupling of radiation to the junctions. (Note that the "sharpness" of the current–voltage characteristics of the lower and higher current-density devices in Fig. 5 is effectively the same, after correcting for the series resistance in their wiring layers—$dV_{\mathrm{gap}} \sim 0.1$–0.2 mV.)

This conclusion is supported by an analysis of the heterodyne performance of the twin-junction tuning circuit. In this analysis, each of the microstrip transmission-line sections in the RF

tuning circuit is replaced by a π-matrix lumped-element circuit model, and the coupling of LO power to the two junctions is then determined in an iterative calculation that takes into account the dependence of the junction admittances on the absorbed LO powers. Given the (different) LO power coupling to the two junctions, the junctions are then replaced by three-port Tucker admittance and noise correlation matrices [24] in order to generate a three-port model for the complete tuning circuit, from which the frequency-dependent mixer noise and gain can be determined. This model of the two-junction tuning circuit is similar to those developed previously in [25] and [26].

In order to evaluate the impact of the junction quality and current density on the mixer noise, the junction model is modified by adding a parallel resistance to the measured current-voltage characteristic of a junction with $J_c = 6.5$ kA/cm^2 and $R_{2.0\,\mathrm{mV}}/R_\mathrm{N} = 60$, and then scaling the voltage and current to obtain the desired gap voltage and junction resistance. (Note that adding this parallel resistance does not change the "sharpness" of the current step and the junction's gap voltage, as is the case in the mixers discussed here.) Finally, the shot noise that is produced by this "excess leakage current" is multiplied by the bias-voltage-dependent factor that was developed in [27] and [28] to account for the amplification of shot noise by multiple Andreev reflection in the leakage current of "leaky" SIS junctions (this factor is $\sim$2.3 at $V_\mathrm{bias} = 2.2$ mV).

Receiver noise temperatures are calculated from the calculated mixer noise temperatures and gains by adding input optical losses that are representative of those in the experimental test setup that is being used, plus an IF system with an input noise temperature of 10 K and a 2 K physical temperature. A 10 K IF system noise temperature is used because it is representative of the 4–8-GHz IF system in the HIFI instrument, in which thermal and mechanical constraints have driven the use of a relatively long stainless steel semi-rigid cable between the mixer (at 2 K) and the cryoamplifier (at 15 K), plus two isolators (one at each end of the long cable).

Fig. 9 presents a comparison of the measured and calculated RF coupling, receiver noise, and receiver conversion gain for two 0.88-THz devices with different junction resistances and tuning circuit dimensions (devices c78-A and c87-A). Because the tuning circuit dimensions and material properties are not known with absolute certainty, the tuning circuit dimensions have been fine-tuned to match the frequency dependence of the calculated RF coupling efficiencies to the measured direct-detection sensitivities (applying the same corrections to the geometries of both devices). Furthermore, an additional lossy element is added to the model to fit the calculated noise temperatures to the measured results. For the sake of argument, this excess loss (and the noise that it generates) is represented as a 2.8-dB loss in front of the mixer, at a physical temperature of 2 K. As is seen in Fig. 9, the result is a reasonably consistent match between the measured and calculated receiver noise temperatures for the two mixers. The fact that the calculated receiver conversion gain of c78-A is somewhat lower than the measured gain indicates that at least part of the observed excess receiver noise is likely due to "warm" losses. (Note that the 2.8 dB of excess loss at 2 K that is assumed in Fig. 9 can be replaced by 1.1 dB of excess loss at 300 K.)
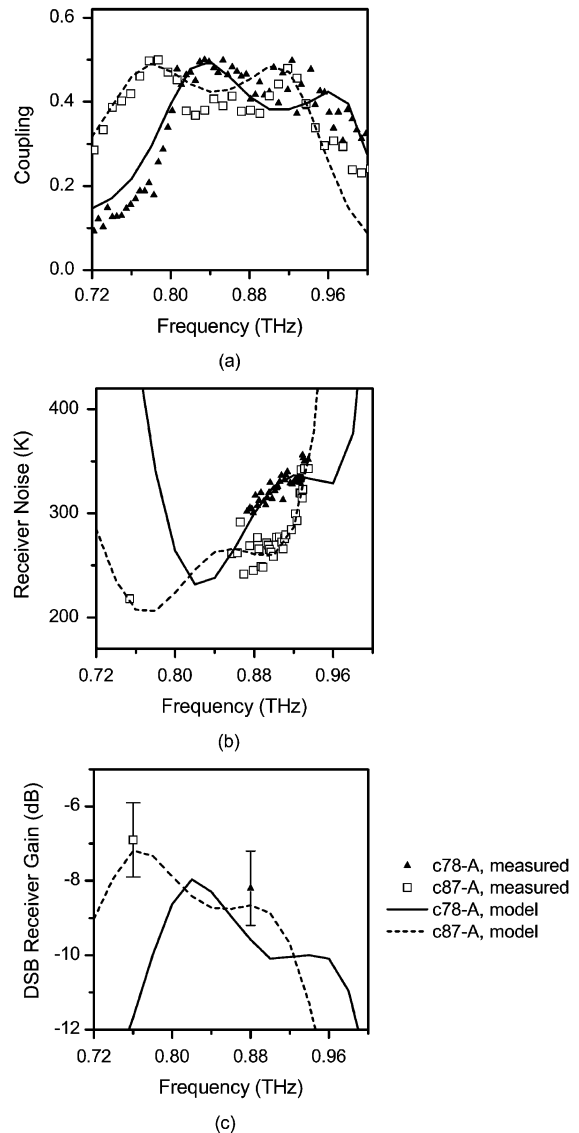

Fig. 9. Comparison of the measured and calculated direct-detection sensitivities, receiver noise temperatures, and DSB receiver conversion gains for devices c78-A and c87-A from the low-J_c 0.88-THz mixer (with $J_c = 6.5$ kA/cm^2 and $R_{2.0\,\mathrm{mV}}/R_\mathrm{N} = 60$). Note that the tuning circuit dimensions in the calculations have been tuned slightly to match the frequency dependences of the measured direct-detection sensitivities. Matching the calculated receiver noise temperatures to the measured values requires that an excess loss be inserted in the model (i.e., 2.8 dB in front of the mixer, at a physical temperature of 2 K). The receiver conversion gain values have been corrected for the gain of the receiver's IF system (the error bars in the measured conversion gains stem from uncertainties in estimating this IF system gain).

The calculated excess noise/loss may originate from a number of sources, including the 77 K blackbody load not being perfectly black (although previous measurements show that it should have an emissivity of $\varepsilon \sim 0.95$ [22]); excess losses in the receiver optics; losses in the corrugated horn, waveguide, and/or substrate channel due to manufacturing errors and/or resistive losses that are not included in the model; dielectric losses in the fused quartz substrate and/or the SiO$_2$ dielectric layer in the tuning circuit, both of which are assumed to be lossless; excess resistive losses in the Al wiring layer and/or the NbTiN ground plane; resistive losses in the Nb junction electrodes (which are not taken into account in this model, but
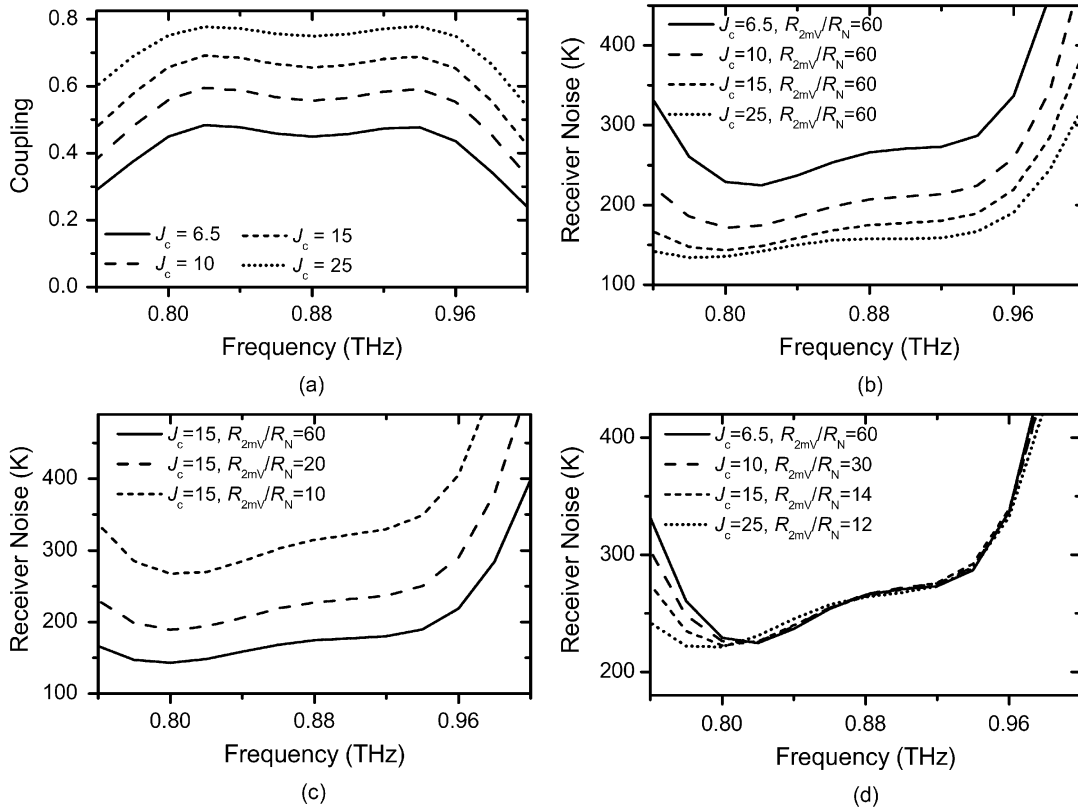
Fig. 10. Calculated sensitivities of 0.88-THz SIS mixers with twin-junction NbTiN/SiO$_2$/Al tuning circuits and junction current densities ranging from 6.5 to 15 kA/cm^2. The same noise and gain contributions for the receiver optics and IF system that were used in Fig. 9 are used in these calculations (including the 2.8-dB excess loss in front of the mixer). (a) Frequency dependence of the direct-detection coupling to the SIS junctions for different current densities. (b) and (c) Frequency dependence of the DSB receiver noise for different combinations of current density and junction quality ($R_{2.0 \, mV}/R_N$). (d) Frequency dependence of the DSB receiver noise for different current densities, with the junction quality being defined at each current density as the value that is needed to obtain the same sensitivity as is obtained with $J_c = 6.5$ kA/cm^2 and $R_{2.0 \, mV}/R_N = 60$. A mixer bias voltage of 2.2 mV is used for all calculations, which is close to the optimum in all cases, while the input noise of the IF system is assumed to be 10 K, which is representative of the 4–8-GHz IF system in the HIFI instrument. For each combination of current density and junction quality, a frequency-independent LO power is used that optimizes the average noise temperature across the 0.8–0.96-THz band.

which are present); and impedance mismatches and/or resistive losses in the mixer's IF circuit (which is represented by a 50 Ω load and an input noise of 10 K).

B. Junction Current Density and Quality Versus Receiver Noise

Using the previously described receiver noise model of the twin-junction mixer, including the 2.8-dB excess loss term that was determined from the results in Fig. 9, the receiver noise of the 0.88-THz mixer has been calculated as a function of junction current density and quality (while adjusting the junction size and the dimensions of the tuning circuit's transformer section to optimize the average RF coupling efficiency over the 0.8–0.96-THz band for each case). The results of these calculations are summarized in Fig. 10.

Note that, for each combination of current density and junction quality, the LO power level has been adjusted to optimize the average sensitivity across the band. (Within the 0.8–0.96-THz band, the sensitivities offered by these "averaged" optimum LO powers do not vary significantly from those that are obtained if the LO power is optimized at each frequency.) The optimum LO power thus increases with both current density and leakage current, although the increase in LO power with current density is driven by a corresponding

reduction in junction resistance—the pumping level of the junction, as measured by the alpha parameter ($\alpha = eV_{LO}/hf$), does not change significantly with current density. A bias voltage of 2.2 mV is used for all calculations—this value is close to the optimum in all cases.

Not surprisingly, it is seen that, if the junction quality ($R_{2.0 \, mV}/R_N$) remains constant, then the receiver noise temperature drops significantly with increasing current density [see Fig. 10(b)]. However, experience shows that junction quality drops with increasing current density in high current density ($J_c > 10$–15 kA/cm^2) SIS junctions with AlO$_x$ tunnel barriers. This reduction in junction quality causes a corresponding increase in mixer shot noise [27], [28] that will (partially) offset the improved coupling of incident radiation to the junctions [see Fig. 10(c)]. Indeed, Fig. 10(d) presents the calculated receiver sensitivities for current densities between 6.5 and 15 kA/cm^2, with a junction quality in each case that is defined as the minimum value that is needed for junctions with that current density to offer a receiver sensitivity that is equal to that which is obtained with $J_c = 6.5$ kA/cm^2 and $R_{2.0 \, mV}/R_N = 60$ kA/cm^2.

Reviewing these calculations, it is noted that moving from $J_c = 6.5$ to 10 and 15 kA/cm^2 requires that junction qualities of at least $R_{2.0 \, mV}/R_N = 30$ and 14, respectively, are maintained
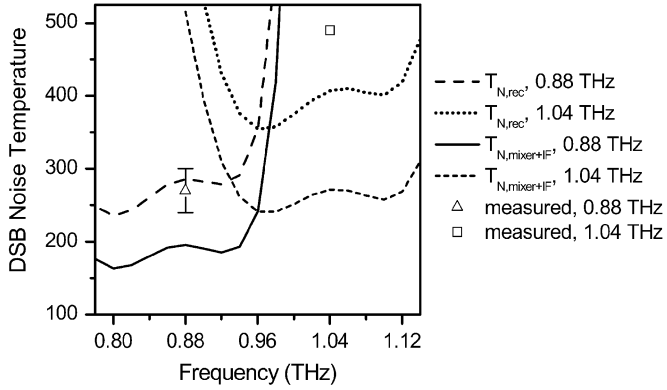
Fig. 11.   Calculated receiver and mixer sensitivities ($T_{\mathrm{N,rec}}$ and $T_{\mathrm{N,mixer+IF}}$) for 0.88- and 1.04-THz mixers with current densities of $J_c = 6.5$ kA/cm^2 and junction qualities of $R_{2.0\ \mathrm{mV}}/R_{\mathrm{N}} = 60$. The lower sensitivity of the 1.04-THz mixers is due to a combination of the increased operating frequency (which increases the noise contributions of RF coupling losses and reduces the intrinsic conversion efficiency of the junctions) and the reduced coupling efficiency of the tuning circuit (due to the use of a NbTiN ground plane with a higher conductivity, and thus a smaller penetration depth). (Due to the reduced penetration depth of the NbTiN ground plane deposited at 400 °C, the microstrip sections need to be made longer and narrower to keep the same electrical length and impedance, which increases the series resistance in the Al wiring layer.) For reference, indicators of the measured receiver sensitivities of the 0.88- and 1.04-THz mixers presented in Fig. 8 are also included.

in order to not lose receiver sensitivity. What is particularly interesting about this result is the fact that it is consistent with the observation that no significant difference is seen in the heterodyne performances of mixers with $J_c = 6.5$ and 13 kA/cm^2 and $R_{2.0\ \mathrm{mV}}/R_{\mathrm{N}} = 60$ and 20, respectively. It is also interesting to note that these calculations are also in qualitative agreement with previous observations [29] that 0.64–0.8-THz mixers with $J_c \sim 7$ kA/cm^2 and $R_{2.0\ \mathrm{mV}}/R_{\mathrm{N}} \sim 20$ yield similar sensitivities as mixers with $J_c \sim 13$ kA/cm^2 and $R_{2.0\ \mathrm{mV}}/R_{\mathrm{N}} \sim 7$.

Note that the increase in the mixers' broad-band sensitivities that is obtained with higher current-density junctions is recognized [see Fig. 10(d)]. However, for the purpose of this comparison, only the sensitivities in the 0.8–0.96-THz range are considered.

C. Comparison of the 0.88- and 1.04-THz Results

This twin-junction mixer sensitivity model can also be used to compare the relative sensitivities of the 0.88- and 1.04-THz mixers described in this paper. In particular, Fig. 11 presents the calculated sensitivities of 0.88- and 1.04-THz mixers in which the tuning circuit and junction geometries have been fine-tuned to center the mixers' responses on their respective frequency bands. From this plot, it is seen that a large fraction of the difference in the measured sensitivities of the two mixers is attributable to factors that are included in the previously described mixer noise model. These factors include a drop in the junctions' intrinsic conversion efficiencies and an increase in the noise contributions of optical losses with increasing operating frequency. Additionally, because the penetration depth in NbTiN films deposited at 400 °C is expected to be smaller than that of films deposited at room temperature (due to their significantly higher

normal-state conductivities), the characteristic impedance of a given width of NbTiN/SiO$_2$/Al microstrip transmission line is reduced. As a result, maintaining the impedance and electrical lengths of the microstrip sections in the tuning circuit requires that they be made longer and narrower when replacing a room-temperature-deposited film with one deposited at 400 °C, which increases the series resistance of the Al wiring layer. Finally, it is noted that the 1.04-THz devices presented here are characterized by a series resistance in their current–voltage characteristics that is a factor of two higher than that in the 0.88-THz devices. This is a sign that the low-temperature resistivity of the Al wiring layer is likely higher in these devices than the $\rho_{\mathrm{Al},4\mathrm{K}} \sim 0.5\ \mu\Omega \cdot$ cm that is realized in the 0.88-THz devices. If this factor-of-two increase in the resistivity of the Al wiring layer is included in the noise model for the 1.04-THz mixer, the calculated receiver noise increases by $\sim 10\%$ across the band, which brings it much closer to the $T_{\mathrm{N,rec}} = 500$ K that is obtained with device f49–C at 1.04 and 1.14 THz.

VIII. CONCLUSION

The development of SIS mixer devices incorporating NbTiN/SiO$_2$/Al microstrip tuning circuits and a parallel pair of "standard" 1–μm^2 Nb/Al-AlO$_x$/Nb SIS junctions has enabled the development of low-noise mixers in the 0.8–1.12-THz range. Furthermore, the use of half-height 0.88- and 1.04-THz waveguide embedding geometries and the optimization of SIS devices to couple efficiently to these embedding circuits has yielded low receiver noise temperatures across the 0.8–0.96- and 0.96–1.12-THz bands of the HIFI instrument; a high-resolution heterodyne spectrometer that is being built for the European Space Agency's Herschel Space Observatory.

Analyzing the measured mixer performance with a three-port admittance and noise model of the SIS tuning circuit (in which three-port "Tucker" models of the SIS junctions are combined with lumped-element representations of the microstrip transmission lines), it is found that the frequency dependence of the measured performance is consistent with calculations, but that the measured noise can only be reproduced by inserting 2.8 dB of excess loss into the noise model (in front of the mixer, at a physical temperature of 2 K). The calculated results are also consistent with the observation that mixers containing junctions with current densities of $J_c = 6.5$ and 13 kA/cm^2 yield similar sensitivities. This may be attributed to the fact that the improved RF coupling that is obtained with higher current-density junctions is offset by an increase in junction shot-noise (due to the fact that the higher current-density junctions have larger leakage currents—$R_{2.0\ \mathrm{mV}}/R_{\mathrm{N}} \sim 20$ for $J_c = 13$ kA/cm^2 versus $R_{2.0\ \mathrm{mV}}/R_{\mathrm{N}} = 30$–60 for $J_c = 6.5$ kA/cm^2).

Finally, a significant fraction of the drop in sensitivity of the 1.04-THz devices relative to the 0.88-THz devices is attributed to the intrinsic effects of the higher operating frequency (which causes the conversion gains of the SIS junctions to drop and the noise contributions of RF losses to increase) and the smaller penetration depth in the "higher quality" NbTiN films used in these devices.

REFERENCES

[1] T. de Graauw and F. P. Helmich, "Herschel-HIFI: The heterodyne instrument for the far infrared," in *SP-460 The Promise of the Herschel Space Observatory*, G. L. Pilbratt, J. Cernicharo, A. M. Heras, T. Prusti, and R. A Harris, Eds. Noordwijk, The Netherlands: ESA Pub. Div., 2001, pp. 45–52.

[2] G. L. Pilbratt, J. Cernicharo, A. M. Heras, T. Prusti, and R. A Harris, *SP-460 The Promise of the Herschel Space Observatory*. Noordwijk, The Netherlands: ESA Pub. Div., 2001.

[3] J. W. Kooi, M. Chan, B. Bumble, H. G. LeDuc, P. Schaffer, and T. G. Phillips, "230 and 492 GHz low noise SIS waveguide receivers employing tuned Nb/AlO$_x$/Nb tunnel junctions," *Int. J. Inf. Millim. Waves*, vol. 16, pp. 2049–2068, Dec. 1995.

[4] A. Karpov, J. Blondel, M. Voss, and K. H. Gundlach, "A three photon noise SIS heterodyne receiver at submillimeter wavelength," *IEEE Trans. Appl. Supercond.*, vol. 9, no. 6, pp. 4456–4459, Jun. 1999.

[5] C. E. Honingh, S. Haas, D. Hottgenroth, K. Jacobs, and J. Stutzki, "Low noise broadband fixed tuned SIS waveguide mixers at 660 and 800 GHz," *IEEE Trans. Appl. Supercond.*, vol. 7, no. 6, pp. 2582–2586, Jun. 1997.

[6] D. C. Mattis and J. Bardeen, "Theory of the anomalous skin effect in normal and superconducting metals," *Phys. Rev.*, vol. 111, pp. 412–417, 1958.

[7] G. de Lange, J. J. Kuipers, T. M. Klapwijk, R. A. Panhuyzen, H. van de Stadt, and M. W. M. de Graauw, "Superconducting resonator circuits at frequencies above the gap frequency," *J. Appl. Phys.*, vol. 77, pp. 1795–1804, Feb. 1995.

[8] J. Kawamura, J. Chen, D. Miller, J. Kooi, J. Zmuidzinas, B. Bumble, H. G. Leduc, and J. A. Stern, "Low-noise submillimeter-wave NbTiN superconducting tunnel junction mixers," *Appl. Phys. Lett.*, vol. 75, pp. 4013–4015, Dec. 1999.

[9] B. D. Jackson, A. M. Baryshev, G. de Lange, S. V. Shitov, J.-R. Gao, N. N. Iosad, and T. M. Klapwijk, "Low-noise 1 THz superconductor-insulator-superconductor mixer incorporating a NbTiN/SiO$_2$/Al tuning circuit," *Appl. Phys. Lett.*, vol. 79, pp. 436–438, Jul. 2001.

[10] B. D. Jackson, N. N. Iosad, G. de Lange, A. M. Baryshev, W. M. Laauwen, J.-R. Gao, and T. M. Klapwijk, "NbTiN/SiO$_2$/Al tuning circuits for low-noise 1 THz SIS mixers," *IEEE Trans. Appl. Supercond.*, vol. 11, no. 3, pp. 653–656, Mar. 2001.

[11] B. D. Jackson, G. de Lange, T. Zijlstra, M. Kroug, T. M. Klapwijk, and J. A. Stern, "Niobium titanium nitride based superconductor-insulator-superconductor mixers for low-noise THz receivers," *J. Appl. Phys.*, vol. 97, no. 11, p. 113 904 1–8, Jun. 2005.

[12] G. de Lange, B. Jackson, T. Zijlstra, M. Kroug, and T. M. Klapwijk, "Development of the band 3 and 4 mixer units for HIFI," in *Millimeter and Submillimeter Detectors for Astronomy, Proc. of the SPIE*, J. Zmuidzinas, W. S. Holland, and S. Withington, Eds. Bellingham, WA: SPIE, 2004, vol. 5498, pp. 268–277.

[13] J. W. Kooi, private communication, 2000–2003.

[14] B. D. Jackson, G. de Lange, W. M. Laauwen, L. de Jong, T. Zijlstra, N. N. Iosad, and T. M. Klapwijk, "THz SIS mixer development for HIFI," in *Proc. 13th Int. Symp. Space THz Technol.*, R. Blundell and E. Tong, Eds. Cambridge, MA, 2002, pp. 561–570.

[15] H. van de Stadt, H. Scheaffer, and L. de Jong, private communication, 1996–1998.

[16] A. M. Baryshev, H. van de Stadt, H. Schaeffer, R. Hesper, T. Zijlstra, M. Zuiddam, W. Wild, and L. de Jong, "Development of a 0.6 THz SIS receiver for ALMA," in *Proc. 12th Int. Symp. Space THz Technol.*, I. Mehdi, Ed.. San Diego, CA, 2001, pp. 581–590.

[17] R. L. Eisenhart and P. J. Khan, "Theoretical and experimental analysis of a waveguide mounting structure," *IEEE Trans. Microw. Theory Tech.*, vol. MTT-19, no. 8, pp. 706–719, Aug. 1971.

[18] C.-Y. E. Tong, R. Blundell, S. Paine, D. C. Papa, J. Kawamura, X. Zhang, J. A. Stern, and H. G. LeDuc, "Design and characterization of a 250–350-GHz fixed-tuned superconductor-insulator-superconductor receiver," *IEEE Trans. Microw. Theory Tech.*, vol. 44, no. 9, pp. 1548–1556, Sep. 1996.

[19] J. A. Stern, B. Bumble, H. G. Leduc, J. W. Kooi, and J. Zmuidzinas, "Fabrication and dc-characterization of NbTiN based SIS mixers for use between 600 and 1200 GHz," in *Proc. 9th Int. Symp. Space THz Technol.*, R. McGrath, Ed.. Pasadena, CA, 1998, pp. 305–313.

[20] H. B. Callen and T. A. Welton, "Irreversibility and generalized noise," *Phys. Rev.*, vol. 83, pp. 34–40, 1951.

[21] T. O. Klaassen, M. C. Diez, J. H. Blok, C. Smorenburg, K. J. Wildeman, and G. Jakob, "Optical characterization of absorbing coatings for submillimeter radiation," in *Proc. 12th Int. Symp. Space THz Technol.*, I. Mehdi, Ed., San Diego, CA, 2001, pp. 400–409.

[22] N. D. Whyborn, private communication, Jul. 2005.

[23] I. Lopez-Fernandez, J. D. G. Puyol, A. B. Cancio, and F. Colomer, "New trends in cryogenic HEMT amplifiers for radio astronomy," presented at the Int. Science and Technology Meeting on the Square Kilometer Array, Berkeley, CA, Jul. 9–13, 2001.

[24] J. R. Tucker and M. J. Feldman, "Quantum detection at millimeter wavelengths," *Rev. Mod. Phys.*, vol. 57, pp. 1055–1113, Oct. 1985.

[25] J. Zmuidzinas, H. G. Leduc, J. A. Stern, and S. R. Cypher, "Two-junction tuning circuits for submillimeter SIS mixers," *IEEE Trans. Microw. Theory Tech.*, vol. 42, no. 4, pp. 698–706, Apr. 1994.

[26] T. Noguchi, S. C. Shi, and J. Inatani, "Parallel connected twin SIS junctions for millimeter and submillimeter-wave mixers—Analysis and experimental verification," *IEICE Trans. Elect.*, vol. E78C, pp. 481–489, May 1995.

[27] P. Dieleman, H. G. Bukkems, T. M. Klapwijk, M. Schicke, and K. H. Gundlach, "Observation of Andreev reflection enhanced shot noise," *Phys. Rev. Lett.*, vol. 79, pp. 3486–3489, Nov. 1997.

[28] P. Dieleman and T. M. Klapwijk, "Shot noise beyond the Tucker theory in niobium tunnel junction mixers," *Appl. Phys. Lett.*, vol. 72, pp. 1653–1655, Mar. 1998.

[29] R. Teipen, M. Justen, T. Tils, S. Glenz, C. E. Honingh, K. Jacobs, B. D. Jackson, T. Zijlstra, and M. Kroug, "Influence of junction-quality and current density on HIFI band 2 mixer performance," in *Proc. 14th Int. Symp. Space THz Technol.*, C. Walker and J. Payne, Eds., Tucson, AZ, 2003, pp. 55–62.

Brian D. Jackson received the B.A.Sc. degree in engineering physics from the University of British Columbia, Vancouver, BC, Canada, in 1995, the M.S. degree in electrical and computer engineering from the University of Toronto, Toronto, ON, Canada, in 1997, and the Ph.D. degree in applied physics from the Delft University of Technology, Delft, The Netherlands, in 2005.

He was a Research Assistant with the National Research Council of Canada, Ottawa, ON, Canada, in 1995, and with the University of Toronto from 1995 to 1997. From 1997 to 1999, he was a Research Engineer with the University of Groningen, Groningen, The Netherlands. Since 1999, he has been an Instrument Scientist with the SRON Netherlands Institute for Space Research, Groningen, The Netherlands. His main research activities are in the areas of SIS junction and mixer development for radio astronomy and system engineering for heterodyne instruments for space- and ground-based telescopes. He has played a role in SIS mixer and/or receiver development for the James Clerk Maxwell Telescope, the Heterodyne Instrument for the Far-Infrared (HIFI) on the European Space Agency's Herschel Space Observatory, and for the Atacama Large Millimeter Array.

Gert de Lange received the M.S. and Ph.D. degree from the University of Groningen, Groningen, The Netherlands, in 1988 and 1994, respectively, both in applied physics.

From 1994 to 1998, he was a Research Scientist with the Massachussetts Institute of Technology, Cambridge, working on the development of superconducting micromachined heterodyne detector arrays. Since 1998, he has been an Instrument Scientist with the SRON Netherlands Institute for Space Research, Groningen, The Netherlands. His main research activities are in the areas superconducting detector development for low-noise heterodyne receivers for space- or ground-based and airborne submillimeter astronomical instrumentation and the development of space qualified mixer units for the Heterodyne Instrument for the Far-Infrared (HIFI) on the European Space Agency's Herschel Space Observatory.

Tony Zijlstra, photograph and biography not available at the time of publication.

Matthias Kroug, photograph and biography not available at the time of publication.

Jacob W. Kooi, photograph and biography not available at the time of publication.

Jeffrey A. Stern received the B.S. degree in physics from Rensselaer Polytechnic Institute, Troy, NY, in 1983, and the Ph.D. degree in applied physics from the California Institute of Technology, Pasadena, in 1991.

Since receiving his doctorate, he has been with the Jet Propulsion Laboratory, Pasadena, most recently as a Senior Member of the Technical Staff. His work has focused on a number of superconducting sensors including Nb NbTiN and NbN SIS mixers, NbN and NbTiN phononcooled, hot-electron mixers, and, more recently, NbN single0photon detectors. He was in charge of fabricating, space qualifying, and delivering mixer chips for band 5 of the HIFI instrument on Hershel. He has also been involved in delivering SIS mixer chips to the Caltech Millimeter Array and the Harvard Smithsonian Submillimeter Array. He has also delivered 1.4 THz NbTiN HEB mixers for the Harvard Smithsonian Receiver Lab Telescope in Chile.

Teun M. Klapwijk received the Ph.D. degree in applied physics from the Delft University of Technology, Delft, The Netherlands, in 1977. His doctoral degree was entitled "Superconducting Microbridges and Radiation Stimulated Superconductivity."

After receiving the doctorate degree, he continued his research with Delft University as an Assistant/Associate Professor, interrupted by periods as a Research Fellow with Harvard University (1979–1980) and as a Summer-Faculty member with the IBM T. J. Watson Research Laboratory, Yorktown Heights, NY (1983). In 1985, he became a Full Professor with the University of Groningen, where he was involved with silicon MOSFETs, superconductor/semiconductor hybrids, and began his long-term collaboration with the SRON Netherlands Institute of Space Research on heterodyne detection with superconducting tunnel junctions and hot-electron bolometers. This research has found its application at the James Clerk Maxwell Telescope, for the Herschel Space Telescope and the Atacama Large Millimeter Array. In 1999, he returned to Delft University, transferring a portion of his ongoing research program and moving into new areas such a superconducting/ferromagnetic hybrids. He is currently a Professor of applied physics, specializing in the field of nanoelectronics, with the Faculty of Applied Sciences, Kavli Institute of Nanoscience, Delft University of Technology, Delft, The Netherlands. He has authored or coauthored over 250 refereed scientific publications.

Prof. Klapwijk has been an elected Fellow of the American Physical Society since 2001.